

Sudden change in entanglement Hamiltonian: Phase diagram of an Ising entanglement Hamiltonian

Zhe Wang,^{1,2} Siyi Yang,^{3,1,2} Bin-Bin Mao,⁴ Meng Cheng,^{5,*} and Zheng Yan^{1,2,†}

¹*Department of Physics, School of Science and Research Center for
Industries of the Future, Westlake University, Hangzhou 310030, China*

²*Institute of Natural Sciences, Westlake Institute for Advanced Study, Hangzhou 310024, China*

³*State Key Laboratory of Surface Physics and Department of Physics, Fudan University, Shanghai 200438, China*

⁴*School of Foundational Education, University of Health and Rehabilitation Sciences, Qingdao 266000, China*

⁵*Department of Physics, Yale University, New Haven, CT 06520-8120, USA*

The form of the entanglement Hamiltonian varies with the parameters of the original system. Whether there is a singularity is the key problem for demonstrating/negating the universality of the relation between the entanglement spectrum and edge energy spectrum. We carefully study the phase diagram of a 1D Ising entanglement Hamiltonian as an example to clarify the long-standing controversy of the general relation between the entanglement Hamiltonian and original Hamiltonian. Interestingly, even if the singularities indeed exist, the Li-Haldane-Poilblanc conjecture, i.e., the general relation between the entanglement spectrum and edge energy spectrum, seemingly still holds.

Introduction.— Quantum information science and condensed matter physics have rapidly converged and influenced each other in recent years [1, 2]. Within this trend, quantum entanglement was employed to reveal fundamental structures, such as field-theoretical and topological properties, of quantum many-body systems [3–6]. For instance, the entanglement entropy (EE) has become an important tool to characterize topological states and conformal field theories (CFT) [7–22]. Beyond the EE, Li and Haldane proposed that the entanglement spectrum (ES) is a more organic entanglement characteristic to study the intrinsic information of many-body systems [23–25]. Thereafter, low-lying ES has been widely used as a key signature to investigate CFT and topological order in highly entangled quantum matter [26–45].

Going beyond EE and ES, the concept of entanglement Hamiltonian (EH) was also proposed to better describe the structure of bipartite entanglement. Its definition is $H_E = -\ln(\rho_A)$, where the ρ_A is the reduced density matrix (RDM). Both EE and ES can be understood as some observables of the EH at certain temperature. In this sense, the EH can be treated as an even more basic physical quantity and is highly worthy to be carefully studied. Recently, further detailed studies have analyzed the EH based on field theory, numerics, and experiment [46–62].

The correspondence between the EH and the original Hamiltonian (OH) is still a charming puzzle that hasn't been completely solved yet. The famous Li-Haldane-Poilblanc (LHP) conjecture [23, 25] posited that the EH always resembles the OH on the virtual edge. Furthermore, the Bisognano-Wichmann (BW) theorem gives the form of the EH based on its OH, but it only holds under some strict conditions, e.g., the entanglement region has no corner, the low-energy theory is a relativistic quantum field theory [63–66]. In both cases (i.e. when the LHP conjecture holds, or when the BW theorem applies), the EH should change smoothly when continuously tuning

the parameter of the original Hamiltonian.

However, Chandran, Khemani and Sondhi argued that the EH could have singularities at quantum critical points (QCP) of the original Hamiltonian [67]. A straightforward example they proposed is a discussion about the EH of a 2D transverse field Ising model (TFIM) with half-cutting. In their argument, according to the Mermin-Wagner (MW) theorem [68, 69], the system of EH can not be ordered except at $T_E = 0$ (temperature for the EH) in the paramagnetic (PM) phase of the OH because the EH of a 2D TFIM is a 1D Ising-like system [70]. However, at $T_E \geq 1$, the system of the EH presents an Ising order in the ordered phase of the OH (i.e., the TFIM). Notice that $\rho_A = e^{-H_E}$ can be treated as the ensemble of H_E at $T_E = 1$. Meanwhile, the physical property of this ensemble should be same as the ground state of the original Hamiltonian.

In the above analysis, the system of the EH in PM side of the OH must be disordered when $T_E > 0$ and is ordered in the Ising side in the region $T_E \leq 1$, thus the EH here should display a discontinuity at the QCP of the original Hamiltonian. While physically reasonable, the argument relies on approximations that are not fully justified. For example, the EH was derived in the strong coupling limit by first-order perturbation theory, which is shown to be short range. However, near the QCP (corresponding to the thermal phase transition of the EH), the long-range part of the interactions of the EH should be significantly enhanced [71], which are not captured by the perturbative analysis.

Meanwhile, the importance of long-range interactions was highlighted by a recent numerical work [58]. It was shown that, the long-range terms of the EH can indeed change the underlying physics, e.g., violating the Mermin-Wagner theorem. This motivates a thorough investigation of long-range interactions and the corresponding phase diagram of the EH within a concrete lat-

tice model. In this paper, we take up this challenge by studying a quantum Ising model through both numerical calculations and theoretical analysis. Our results provide new insights into the nature of the ES and confirm that the universal features of the ES remain robust, even under these modifications.

The models and methods.- The system we discussed here is a spin-1/2 ladder [Fig. 1(a)], with intra-chain ferromagnetic (FM) Ising interactions, and inter-chain antiferromagnetic (AFM) Heisenberg interactions. The Hamiltonian is given by

$$H_H = J_H \sum_i S_{i,1} \cdot S_{i,2} + J_I \sum_{l=1,2} \sum_i S_{i,l}^y \cdot S_{i+1,l}^y \quad (1)$$

where $l = 1, 2$ denote the two legs of the ladder, $J_H > 0$ is the inter-chain AFM Heisenberg exchange interaction, and $J_I < 0$ is the intra-chain FM Ising interaction. This model can be efficiently simulated by a cluster Stochastic Series Expansion (SSE) algorithm [62, 72–74].

We will also consider a variant of Eq.(1), where the inter-chain interactions are XY-like:

$$H_{XY} = -J_{XY} \sum_i (S_{i,1}^x \cdot S_{i,2}^x + S_{i,1}^y \cdot S_{i,2}^y) + J_I \sum_{l=1,2} \sum_i S_{i,l}^y \cdot S_{i+1,l}^y \quad (2)$$

The advantage of this model is that the reduced density matrix can be found exactly, thus facilitating a more systematic study of the phase diagram of the EH. The details of the derivation of the reduced density matrix is given in the Supplementary Materials (SM). It is worth noting that both the two models above have similar Ising-like EHS and related physics.

We choose one chain as the environment and the other one as the subsystem to further explore the entanglement property. Via an analysis of the path-integral representation for this class of models [62], the reduced density matrix must be diagonal in the S^z basis, thus the EH is effectively a classical Ising model (with possibly long-range interactions). This is shown explicitly for the second model H_{XY} (see SM for details).

For H_H in Eq.(1), we use the recently developed replica quantum Monte Carlo method [58, 60–62, 75] to study the ensemble of EH. The key point is to simulate a Rényi replica partition-function $Z_A^{(n)} \propto \text{Tr} \rho_A^n = \text{Tr} e^{-nH_E}$. The replica index n here can be considered as the effective inverse temperature $\beta_E = 1/T_E$ of the EH H_E . By simulating different values n , one can effectively tune the temperature of the EH. More details of this method are explained in the SM. Note that in this article, when we talk about β_E , we mean the inverse temperature of EH, and β is the inverse temperature of OH.

Although the replica QMC algorithm can perform large-size simulations, the effective inverse temperature β_E can only take integer values and $\beta_E \geq 1$, which limits

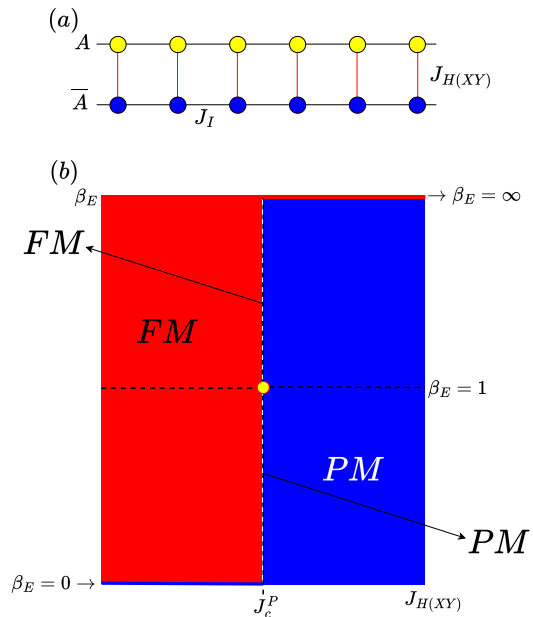


FIG. 1. (a) Ising ladder: the chains with FM Ising exchange interactions J_I coupled by AFM rung Heisenberg couplings J_H or XY-like couplings J_{XY} . We choose the chain with blue sites as environment A and the chain with yellow sites as the subsystem A we concern. (b) Phase diagram of the entanglement Hamiltonian H_E of the original Hamiltonian $H_H(H_{XY})$. The yellow dot at $(J_c^P, \beta_E = 1)$ represents a quantum transition of the original Hamiltonian or thermodynamic phase transitions of the EH. The red region indicates that the system is in the FM phase, and the blue region indicates the paramagnetic (PM) phase. Two long arrows indicate that the dashed line belongs to the FM or PM phase, respectively.

our ability to explore the phase diagram of the entanglement Hamiltonian at high temperature. To this end, the other model Eq.(2), provides a complementary perspective: because the RDM is explicitly known, the EH at any temperature can be studied. However, the high computational complexity of calculating the weights in the reduced density matrix makes that the available system size is smaller than using the replica QMC method. By combining these two methods, we can synthetically explore the phase diagram of the Ising-like entanglement Hamiltonian.

Numerical results.- The phase diagram of the EH can be studied as a function of the inverse temperature β_E of the EH and the coupling $J_H(J_{XY})$ of the OH. First, we note that the two models show qualitatively the same phase diagram, which consists of ferromagnetic (FM) and paramagnetic (PM) phases. The Ising magnetic order can be characterized by the uniform magnetization $m^y = \frac{1}{L} \sum_i S_i^y$ (the FM ordered along the y axis in our models). We define the Ising Binder cumulant

$U_2 = \frac{3}{2} \left(1 - \frac{1}{3} \frac{\langle (m^y)^4 \rangle}{\langle (m^y)^2 \rangle^2} \right)$. It is well-known that in the FM (PM) phase, U_2 converges to 1 (0) with increasing system size. The critical point can be accurately located by analyzing the crossing of U_2 .

Let us start from the the line of $\beta_E = 1$ in the Fig.1 (b). By definition, the phase diagram should be same as the one of the original Hamiltonian. Denote by J_c^P the critical coupling of the OH, the right side of which is the PM phase and the left is FM. By setting $J_I = -1$ in Eq.(1) and $J_I = -1/2$ in Eq.(2), the QCPs of the two models should have same value $J_c^P = 1$. This is confirmed numerically in both models. For H_H , the QMC calculation of U_2 in the ground state is shown in [Fig. 2 (a)]. For H_{XY} , results from the classical MC simulation of the EH are presented in Fig. 2 (c).

At $\beta_E = 1$, the quantum critical point of the OH is equivalent to the thermal critical point of the EH at J_c^P . The existence of such a thermal phase transition implies that the EH at J_c^P must have long range interactions in order to circumvent the Mermin-Wagner theorem. This is further demonstrated directly in explicit form of the EH given by Eq.(2) in the SM.

Having understood the phase diagram along $\beta_E = 1$, we now explore the global phase diagram more systematically. First we consider the neighborhood of the critical point at $\beta_E = 1, J_H(J_{XY}) = J_c^P$. An immediate question arises: away from $\beta_E = 1$, is $J_H(J_{XY}) = J_c^P$ an isolated critical point, or it belongs to a critical line?

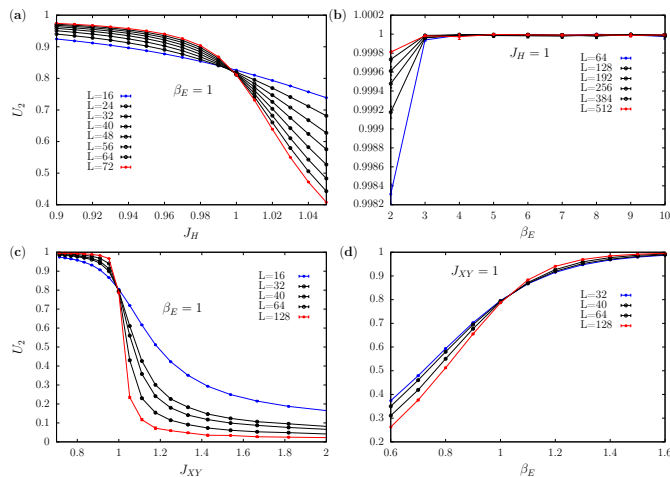


FIG. 2. The Binder cumulant are calculated along two dashed lines passing through QCPs of OH in Fig. 1(b). (a) and (b) are the results of the EH from Hamiltonian H_H . (c) and (d) are the results of the EH from Hamiltonian H_{XY} .

To answer the above question, we fix the $J_H(J_{XY}) = J_c^P = 1$ and tune β_E to study the behavior of the Binder cumulant, as displayed in Fig. 2 (b) and (d). Although the replica method of QMC can only access integer values of $\beta_E \geq 1$, from Fig. 2 (b) we can clearly see that the system (EH of Eq.(1)) is ordered when $\beta_E > 1$. For H_{XY} ,

the analytical form of the EH (Eq.(2)) allows simulations done in whole parameter region, which shows clearly that the thermal phase transition only happens at $\beta_E = 1$ [Fig. 2 (d)]. One can find that the physics shown in (b) is qualitatively similar to the one in the region $\beta_E > 1$ of (d). Both figures support the conclusion that there is a single critical point along the J_c^P line instead of a critical line.

Furthermore, we adopt finite-size scaling $U_2(g, L) = L^{-\kappa} f[(g - g_c)L^{1/\nu}]$ to rescale the Binder cumulant. Here $g = J_H(J_{XY})$ or $T_E = 1/\beta_E$, and ν is correlation length exponent. Using the 2D Ising critical exponent $\nu = 1$, we find that the data (obtained by setting $\beta_E = 1$ and tuning $J_H(J_{XY})$, see horizontal dashed line in Fig. 1 (b)) of U_2 for different system sizes fall onto the same curve (see SM), which means that the critical point on the $\beta_E = 1$ line belongs to the 2D Ising universality class, as expected.

However, the critical exponents become totally different if the critical point is approached along another direction. Setting $J_{XY} = 1$ and tuning β_E (the vertical dashed line at J_c^P in Fig. 1 (b)), U_2 for different system sizes cannot be collapsed to a same curve with $\nu = 1$. If we set ν free to fit the data, the optimal value is $1/\nu = 0.24(1)$. Additionally, we perform scaling collapse for $\langle (m^z)^2 \rangle$ with $\kappa = 2\beta/\nu$ to fit ν and β/ν . We find $\beta/\nu = 0.123(2)$ and $1/\nu = 0.34(2)$. The former is consistent with 2D Ising universality class, while the latter is not. Note that the $1/\nu$ fitted from $(m^z)^2$ is also different from $1/\nu = 0.24(1)$ from the scaling analysis of U_2 above, which may result from finite-size effects. Details about the fitting of critical exponents can be found in SM. The fitting results show β/ν is universal in different parameter paths (β_E or J), while ν is highly dependent on the detailed path. The reason may be either the critical exponents β or ν explicitly includes the effective dimension d of the Hamiltonian, but β/ν is dimensionless.

Now the question becomes whether the EH will turn into a short-range one suddenly when it is moved slightly to the right side of J_c^P . To understand this issue, we fix β_E and scan the parameter $J_H(J_{XY})$ around J_c^P to obtain the Binder cumulant U_2 , as shown in Fig. 3. Via the replica method, the simulated sizes are much larger. Fig. 3 (a) and (b) show that the Binder cumulant has no crossing point and the curve becomes sharper and sharper when the system size increases. Similar results have been shown in the figure (c) and (d) through simulating the analytical EH of OH H_{XY} , although the simulated system sizes are smaller in this approach. Then we choose the parameter points close to J_c^P in both two models, $J_H = 1.1$ and $J_{XY} = 1.05$, to simulate the U_2 in the respective methods. Either figure (e) or (f) has no obvious crossing, which suggests that there is no phase transition at finite temperature. This is consistent with the expectation from the Mermin-Wagner theorem in systems with short-range interactions. Therefore, our

simulation results support the conclusion that there is a sudden change of the EH before the J_c^P , that is, the EH remains short-range until reaching the QCP of the OH.

The numerical results can also be understood theoretically. As the Fig. S2 in the SM show, the form of the analytical EH reflects that all the matrix elements $g(x, L)$ are flat except near edges $x = 0$ or L . The physical meaning of a element $g(x, L)$ is the energy cost between two domain walls with distance x . The flat curve actually represents there is no energy cost when moving a domain wall (if we ignore the edge effect). It is an obvious short-range effect in a 1D Ising chain, which strongly supports the EH here is short-range.

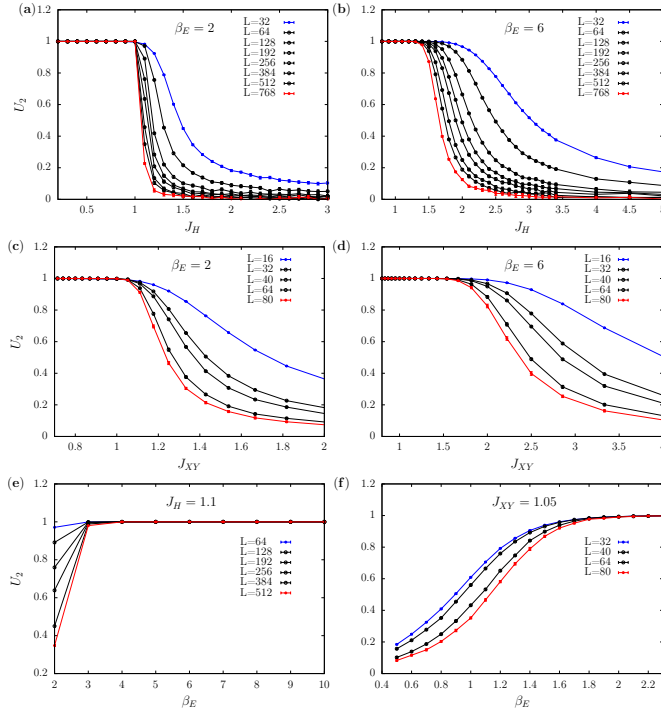


FIG. 3. The Binder cumulant U_2 results of the EH for different L (a) under $\beta_E = 2$ sweeping J_H and (b) under $\beta_E = 6$ sweeping J_H and (c) under $\beta_E = 2$ sweeping J_{XY} and (d) under $\beta_E = 6$ sweeping J_{XY} and (e) under $J_H = 1.1$ sweeping β_E and (f) under $J_{XY} = 1.05$ sweeping β_E . Sweeping J_H (J_{XY}) or β_E , there are no crossings of curves with different L for both systems, which like the 1D Ising model at the finite temperature (see SM). This means no phase transition when focus on OH in the PM phase.

Then the next question is whether the finite temperature phase transition boundary of the FM and PM phases on the left side is continuously connected to the critical point at J_c^P and $\beta_E = 1$ or not? In this case, we need focus on the high temperature region $\beta_E < 1$ where the replica method is powerless, thus we use the classical Monte Carlo to simulate the second EH, Eq.(2), exactly obtained from theoretical analysis. Firstly, we fix the $J_{XY} = 0.95$ and scan the β_E to explore the Binder cumulant crosses, as shown in Fig. 4 (c) and (d). Although

the crossing behaviour was found weakly, the shift of the crossing point of different system sizes are obvious. According to the data extrapolation in the Fig. 4 (f) and SM, the crossing point moves to the $\beta_E = 0$ as $L \rightarrow \infty$, which reveals the FM phase is robust in any finite temperature. We then fix the $\beta_E = 0.1$ and scan the J_{XY} (see Fig. 4 (a) and (b)). Similarly, we can clearly see the drift of the crossing point of different system sizes. According to the data extrapolation in the Fig. 4 (e) and SM, the crossing point tends to the $J_{XY} = 1$. As mentioned above, the EH is in disorder phase at the ($J_{XY} = 1$, $\beta_E = 0.1$), which means there is no phase transition.

Therefore, as shown in Fig. 1, the PM only exists at exactly $\beta_E = 0$ in the region $J < J_c^P$ and FM only lives at strictly $\beta_E = \infty$ in the region $J > J_c^P$.

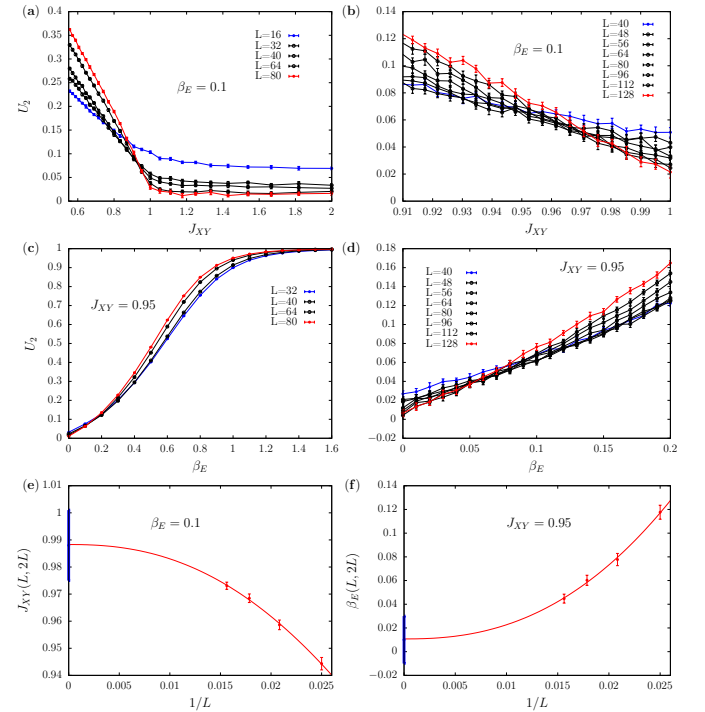


FIG. 4. We focus on the OH of the system H_{XY} in the FM phase. The Binder cumulant U_2 results of the EH for different L (a) under $\beta_E = 0.1$ sweeping J_{XY} and (b) shows more detailed data about (a) and (c) under $J_{XY} = 0.95$ sweeping β_E and (d) shows more detailed data about (c). (e) Fitting about the position of the crossing points of the U_2 curves setting $\beta_E = 0.1$. The blue symbol shows the extrapolated value at the thermodynamic limit, which is 1 within the error bar. (f) Fitting about the position of the crossing points of the U_2 curves setting $J_{XY} = 0.95$. The blue symbol shows the extrapolated value at the thermodynamic limit, which is 0 within the error bar. Details about the fitting see SM.

Discussion and Conclusion. - To summarize, we have systematically studied the full phase diagram of the EH (Ising-like Hamiltonian) obtained from the ground state of the quantum Ising ladder systems. Although for a specific model system, our results shine new light on the

relation between the EH and OH. For example, we now understand that the EH can exhibit abrupt changes even when the OH parameters are varied smoothly. Additionally, long-range interactions can arise suddenly in the EH under certain conditions.

Nevertheless, we observe that the phase diagram is still qualitatively consistent with the LHP conjecture. For example, at the zero temperature $\beta_E = \infty$, the ground state of the EH is always FM, no matter how large $J_H(J_{XY})$ is. This suggests the low-lying excitations of the ES should be similar in the whole parameter region. The LHP conjecture predicts that the ES resembles the low-energy spectrum of Hamiltonian on the virtual edges. In our case, the Hamiltonian of the virtual edge is a single FM Ising chain, thus the low-lying ES always displays the excitation of FM state no matter how the inter-chain coupling changes.

In summary, we have studied the phase diagram of an entanglement Hamiltonian in detail for the first time via solid numerical simulation combined with exactly theoretical solution. The sudden changes of the EH along the parameter $J_H(J_{XY})$ of the OH, emergent long-range interactions in the EH and unusual critical exponents reveal the rich physics in the world of entanglement Hamiltonian. These findings provide deeper insights into the structure of the EH and open new avenues for its exploration.

Acknowledgement. - We acknowledge the start-up funding of Westlake University. The authors also acknowledge Beijing PARATERA Tech Co.,Ltd.(<https://www.paratera.com/>) for providing HPC resources that have contributed to the research results reported within this paper. Z.W. is supported by the China Postdoctoral Science Foundation under Grants No.2024M752898.

* m.cheng@yale.edu

† zhengyan@westlake.edu.cn

- [1] L. Amico, R. Fazio, A. Osterloh, and V. Vedral, Entanglement in many-body systems, *Rev. Mod. Phys.* **80**, 517 (2008).
- [2] N. Laflorencie, Quantum entanglement in condensed matter systems, *Physics Reports* **646**, 1 (2016), quantum entanglement in condensed matter systems.
- [3] G. Vidal, J. I. Latorre, E. Rico, and A. Kitaev, Entanglement in quantum critical phenomena, *Phys. Rev. Lett.* **90**, 227902 (2003).
- [4] V. E. Korepin, Universality of entropy scaling in one dimensional gapless models, *Phys. Rev. Lett.* **92**, 096402 (2004).
- [5] A. Kitaev and J. Preskill, Topological entanglement entropy, *Phys. Rev. Lett.* **96**, 110404 (2006).
- [6] M. Levin and X.-G. Wen, Detecting topological order in a ground state wave function, *Phys. Rev. Lett.* **96**, 110405 (2006).
- [7] P. Calabrese and A. Lefevre, Entanglement spectrum in one-dimensional systems, *Phys. Rev. A* **78**, 032329 (2008).
- [8] E. Fradkin and J. E. Moore, Entanglement entropy of 2d conformal quantum critical points: Hearing the shape of a quantum drum, *Phys. Rev. Lett.* **97**, 050404 (2006).
- [9] Z. Nussinov and G. Ortiz, Sufficient symmetry conditions for Topological Quantum Order, *Proc. Nat. Acad. Sci.* **106**, 16944 (2009).
- [10] Z. Nussinov and G. Ortiz, A symmetry principle for topological quantum order, *Annals Phys.* **324**, 977 (2009).
- [11] H. Casini and M. Huerta, Universal terms for the entanglement entropy in 2+1 dimensions, *Nuclear Physics B* **764**, 183 (2007).
- [12] W. Ji and X.-G. Wen, Noninvertible anomalies and mapping-class-group transformation of anomalous partition functions, *Phys. Rev. Research* **1**, 033054 (2019).
- [13] W. Ji and X.-G. Wen, Categorical symmetry and noninvertible anomaly in symmetry-breaking and topological phase transitions, *Phys. Rev. Research* **2**, 033417 (2020).
- [14] L. Kong, T. Lan, X.-G. Wen, Z.-H. Zhang, and H. Zheng, Algebraic higher symmetry and categorical symmetry: A holographic and entanglement view of symmetry, *Phys. Rev. Research* **2**, 043086 (2020).
- [15] X.-C. Wu, W. Ji, and C. Xu, Categorical symmetries at criticality, *Journal of Statistical Mechanics: Theory and Experiment* **2021**, 073101 (2021).
- [16] J. Zhao, Z. Yan, M. Cheng, and Z. Y. Meng, Higher-form symmetry breaking at ising transitions, *Phys. Rev. Research* **3**, 033024 (2021).
- [17] X.-C. Wu, C.-M. Jian, and C. Xu, Universal Features of Higher-Form Symmetries at Phase Transitions, *SciPost Phys.* **11**, 33 (2021).
- [18] M. Song, J. Zhao, Z. Y. Meng, C. Xu, and M. Cheng, Extracting subleading corrections in entanglement entropy at quantum phase transitions, arXiv preprint arXiv:2312.13498 (2023).
- [19] M. Song, J. Zhao, L. Janssen, M. M. Scherer, and Z. Y. Meng, Deconfined quantum criticality lost, arXiv preprint arXiv:2307.02547 (2023).
- [20] Z. Deng, L. Liu, W. Guo, and H.-q. Lin, Diagnosing $so(5)$ symmetry and first-order transition in the $j - q_3$ model via entanglement entropy, arXiv preprint arXiv:2401.12838 (2024).
- [21] J. D’Emidio and A. W. Sandvik, Entanglement entropy and deconfined criticality: emergent $so(5)$ symmetry and proper lattice bipartition, arXiv preprint arXiv:2401.14396 (2024).
- [22] M. Song, J. Zhao, Y. Qi, J. Rong, and Z. Y. Meng, Quantum criticality and entanglement for the two-dimensional long-range heisenberg bilayer, *Physical Review B* **109**, L081114 (2024).
- [23] H. Li and F. D. M. Haldane, Entanglement spectrum as a generalization of entanglement entropy: Identification of topological order in non-abelian fractional quantum hall effect states, *Phys. Rev. Lett.* **101**, 010504 (2008).
- [24] R. Thomale, D. P. Arovas, and B. A. Bernevig, Nonlocal order in gapless systems: Entanglement spectrum in spin chains, *Phys. Rev. Lett.* **105**, 116805 (2010).
- [25] D. Poilblanc, Entanglement spectra of quantum heisenberg ladders, *Phys. Rev. Lett.* **105**, 077202 (2010).
- [26] F. Pollmann, A. M. Turner, E. Berg, and M. Oshikawa, Entanglement spectrum of a topological phase in one dimension, *Phys. Rev. B* **81**, 064439 (2010).
- [27] L. Fidkowski, Entanglement spectrum of topological insulators and superconductors, *Phys. Rev. Lett.* **104**,

- 130502 (2010).
- [28] H. Yao and X.-L. Qi, Entanglement entropy and entanglement spectrum of the kitaev model, *Phys. Rev. Lett.* **105**, 080501 (2010).
- [29] X.-L. Qi, H. Katsura, and A. W. W. Ludwig, General relationship between the entanglement spectrum and the edge state spectrum of topological quantum states, *Phys. Rev. Lett.* **108**, 196402 (2012).
- [30] E. Canovi, E. Ercolessi, P. Naldesi, L. Taddia, and D. Vodola, Dynamics of entanglement entropy and entanglement spectrum crossing a quantum phase transition, *Phys. Rev. B* **89**, 104303 (2014).
- [31] D. J. Luitz, F. Alet, and N. Laflorencie, Universal behavior beyond multifractality in quantum many-body systems, *Phys. Rev. Lett.* **112**, 057203 (2014).
- [32] D. J. Luitz, F. Alet, and N. Laflorencie, Shannon-rényi entropies and participation spectra across three-dimensional $o(3)$ criticality, *Phys. Rev. B* **89**, 165106 (2014).
- [33] D. J. Luitz, N. Laflorencie, and F. Alet, Participation spectroscopy and entanglement hamiltonian of quantum spin models, *Journal of Statistical Mechanics: Theory and Experiment* **2014**, P08007 (2014).
- [34] C.-M. Chung, L. Bonnes, P. Chen, and A. M. Läuchli, Entanglement spectroscopy using quantum monte carlo, *Phys. Rev. B* **89**, 195147 (2014).
- [35] H. Pichler, G. Zhu, A. Seif, P. Zoller, and M. Hafezi, Measurement protocol for the entanglement spectrum of cold atoms, *Phys. Rev. X* **6**, 041033 (2016).
- [36] J. I. Cirac, D. Poilblanc, N. Schuch, and F. Verstraete, Entanglement spectrum and boundary theories with projected entangled-pair states, *Phys. Rev. B* **83**, 245134 (2011).
- [37] V. M. Stojanović, Entanglement-spectrum characterization of ground-state nonanalyticities in coupled excitation-phonon models, *Phys. Rev. B* **101**, 134301 (2020).
- [38] W.-z. Guo, Entanglement spectrum of geometric states, *Journal of High Energy Physics* **2021**, 1 (2021).
- [39] T. Grover, Entanglement of interacting fermions in quantum monte carlo calculations, *Phys. Rev. Lett.* **111**, 130402 (2013).
- [40] F. F. Assaad, T. C. Lang, and F. Parisen Toldin, Entanglement spectra of interacting fermions in quantum monte carlo simulations, *Phys. Rev. B* **89**, 125121 (2014).
- [41] F. F. Assaad, Stable quantum monte carlo simulations for entanglement spectra of interacting fermions, *Phys. Rev. B* **91**, 125146 (2015).
- [42] F. Parisen Toldin and F. F. Assaad, Entanglement hamiltonian of interacting fermionic models, *Phys. Rev. Lett.* **121**, 200602 (2018).
- [43] X.-J. Yu, R.-Z. Huang, H.-H. Song, L. Xu, C. Ding, and L. Zhang, Conformal boundary conditions of symmetry-enriched quantum critical spin chains, *Phys. Rev. Lett.* **129**, 210601 (2022).
- [44] G. m. H. Roósz and C. Timm, Entanglement of electrons and lattice in a luttinger system, *Phys. Rev. B* **104**, 035405 (2021).
- [45] G. m. H. Roósz and K. Held, Density matrix of electrons coupled to einstein phonons and the electron-phonon entanglement content of excited states, *Phys. Rev. B* **106**, 195404 (2022).
- [46] V. Alba, M. Haque, and A. M. Läuchli, Entanglement spectrum of the heisenberg xxz chain near the ferromagnetic point, *Journal of Statistical Mechanics: Theory and Experiment* **2012**, P08011 (2012).
- [47] W. Zhu, Z. Huang, Y.-C. He, and X. Wen, Entanglement hamiltonian of many-body dynamics in strongly correlated systems, *Phys. Rev. Lett.* **124**, 100605 (2020).
- [48] W. Zhu, Z. Huang, and Y.-C. He, Reconstructing entanglement hamiltonian via entanglement eigenstates, *Physical Review B* **99**, 235109 (2019).
- [49] Q.-C. Tang and W. Zhu, Critical scaling behaviors of entanglement spectra, *Chinese Physics Letters* **37**, 010301 (2020).
- [50] T. Mendes-Santos, G. Giudici, R. Fazio, and M. Dalmonte, Measuring von neumann entanglement entropies without wave functions, *New Journal of Physics* **22**, 013044 (2020).
- [51] M. Dalmonte, V. Eisler, M. Falconi, and B. Vermersch, Entanglement hamiltonians: From field theory to lattice models and experiments, *Annalen der Physik* **534**, 10.1002/andp.202200064 (2022).
- [52] M. K. Joshi, C. Kokail, R. van Bijnen, F. Kranzl, T. V. Zache, R. Blatt, C. F. Roos, and P. Zoller, Exploring large-scale entanglement in quantum simulation, *Nature* **624**, 539 (2023).
- [53] Q. Redon, Q. Liu, J.-B. Bouhiron, N. Mittal, A. Fabre, R. Lopes, and S. Nascimbene, Realizing the entanglement hamiltonian of a topological quantum hall system (2023), [arXiv:2307.06251 \[cond-mat.quant-gas\]](https://arxiv.org/abs/2307.06251).
- [54] M. Dalmonte, B. Vermersch, and P. Zoller, Quantum simulation and spectroscopy of entanglement hamiltonians, *Nature Physics* **14**, 827 (2018).
- [55] M. Ma, Y. Li, and J. Shang, Multipartite entanglement measures: a review (2023), [arXiv:2309.09459 \[quant-ph\]](https://arxiv.org/abs/2309.09459).
- [56] V. Eisler, G. D. Giulio, E. Tonni, and I. Peschel, Entanglement hamiltonians for non-critical quantum chains, *Journal of Statistical Mechanics: Theory and Experiment* **2020**, 103102 (2020).
- [57] M. Pouranvari and J. Abouie, Entanglement conductance as a characterization of a delocalized-localized phase transition in free fermion models, *Phys. Rev. B* **100**, 195109 (2019).
- [58] C. Li, R.-Z. Huang, Y.-M. Ding, Z. Y. Meng, Y.-C. Wang, and Z. Yan, Relevant long-range interaction of the entanglement hamiltonian emerges from a short-range gapped system, *Phys. Rev. B* **109**, 195169 (2024).
- [59] B.-B. Mao, Y.-M. Ding, and Z. Yan, Sampling reduced density matrix to extract fine levels of entanglement spectrum, *arXiv preprint arXiv:2310.16709* (2023).
- [60] M. Song, J. Zhao, Z. Yan, and Z. Y. Meng, Different temperature dependence for the edge and bulk of the entanglement hamiltonian, *Phys. Rev. B* **108**, 075114 (2023).
- [61] Z. Yan and Z. Y. Meng, Unlocking the general relationship between energy and entanglement spectra via the wormhole effect, *Nature Communications* **14**, 2360 (2023).
- [62] S. Wu, X. Ran, B. Yin, Q.-F. Li, B.-B. Mao, Y.-C. Wang, and Z. Yan, Classical model emerges in quantum entanglement: Quantum monte carlo study for an ising-heisenberg bilayer, *Phys. Rev. B* **107**, 155121 (2023).
- [63] M. Dalmonte, V. Eisler, M. Falconi, and B. Vermersch, Entanglement hamiltonians: from field theory to lattice models and experiments, *Annalen der Physik* **534**, 2200064 (2022).
- [64] T. Mendes-Santos, G. Giudici, M. Dalmonte, and M. Rajabpour, Entanglement hamiltonian of quantum critical

- chains and conformal field theories, *Physical Review B* **100**, 155122 (2019).
- [65] T. Mendes-Santos, G. Giudici, R. Fazio, and M. Dalmonte, Measuring von neumann entanglement entropies without wave functions, *New Journal of Physics* **22**, 013044 (2020).
- [66] G. Giudici, T. Mendes-Santos, and P. Calabrese, Entanglement hamiltonians of lattice models via the bisognanowichmann theorem, *Physical Review B* **98**, 134403 (2018).
- [67] A. Chandran, V. Khemani, and S. L. Sondhi, How universal is the entanglement spectrum?, *Phys. Rev. Lett.* **113**, 060501 (2014).
- [68] N. D. Mermin and H. Wagner, Absence of ferromagnetism or antiferromagnetism in one-or two-dimensional isotropic heisenberg models, *Physical Review Letters* **17**, 1133 (1966).
- [69] N. D. Mermin, Absence of ordering in certain classical systems, *Journal of Mathematical Physics* **8**, 1061 (1967).
- [70] According to the Mermin-Wagner (MW) theorem, a 1D Ising chain with short range interaction can not be ordered in finite temperature.
- [71] Only in the presence of long-range interactions, the 1D Ising system can violate MW theorem and has a phase transition.
- [72] A. W. Sandvik, Computational studies of quantum spin systems, in *AIP Conference Proceedings*, Vol. 1297 (American Institute of Physics, 2010) pp. 135–338.
- [73] Z. Yan, Y. Wu, C. Liu, O. F. Syljuåsen, J. Lou, and Y. Chen, Sweeping cluster algorithm for quantum spin systems with strong geometric restrictions, *Physical Review B* **99**, 165135 (2019).
- [74] Z. Yan, Global scheme of sweeping cluster algorithm to sample among topological sectors, *Phys. Rev. B* **105**, 184432 (2022).
- [75] Z. Liu, R.-Z. Huang, Z. Yan, and D.-X. Yao, Demonstrating the wormhole mechanism of the entanglement spectrum via a perturbed boundary, *Phys. Rev. B* **109**, 094416 (2024).

Supplemental Material

Derivation of the entanglement Hamiltonian

Consider the following model (for convenience we set $J_I = -\frac{1}{2}$):

$$H = -\frac{1}{2} \sum_{l=1,2} \sum_j S_{j,l}^y S_{j+1,l}^y - J_{XY} \sum_j (S_{j,1}^x S_{j,2}^x + S_{j,1}^y S_{j,2}^y). \quad (\text{S1})$$

Notice that $[H, S_{j,1}^y S_{j,2}^y] = 0$ for all j , so the ground state should reside in the subspace with $S_{j,1}^y = S_{j,2}^y$. Define

$$\tilde{X}_j = S_{j,1}^x S_{j,2}^x, \tilde{Z}_j = S_{j,1}^y, \quad (\text{S2})$$

we find within the subspace (or similarly in any such subspace)

$$H = - \sum_j (\tilde{Z}_j \tilde{Z}_{j+1} + J_{XY} \tilde{X}_j) - J_{XY} L. \quad (\text{S3})$$

This is nothing but the transverse-field Ising (TFI) model. Suppose the ground state wavefunction of the TFI model in the \tilde{Z} basis is $|\psi(s)\rangle$, where s is a bit string. Then the ground state of H is given by

$$|\psi\rangle = \sum_s \psi(s) |s\rangle_1 |s\rangle_2. \quad (\text{S4})$$

Tracing out one chain, e.g. the 2nd chain, we find the reduced density matrix of the first chain being

$$\rho_A = \sum_s |\psi(s)|^2 |s\rangle\langle s|. \quad (\text{S5})$$

Clearly, the entanglement Hamiltonian is fully classical.

To compute $|\psi(s)|^2$, we note that it must satisfy $\psi(s) = \psi(-s)$ due to the Ising symmetry. As a result, $\psi(s)$ only depends on the configuration of domain walls $\tau_j = s_j s_{j+1}$. Using the Kramers-Wannier duality:

$$\tau_j^x = \tilde{Z}_j \tilde{Z}_{j+1}, \tau_{j-1}^z \tau_j^z = \tilde{X}_j, \quad (\text{S6})$$

Note that with PBC we must have $\prod_j \tilde{X}_j = 1$ and $\prod_j \tau_j^x = 1$. It is clear that the (finite-size) ground state of the transverse-field Ising chain always has $\prod_j \tilde{X}_j = 1$.

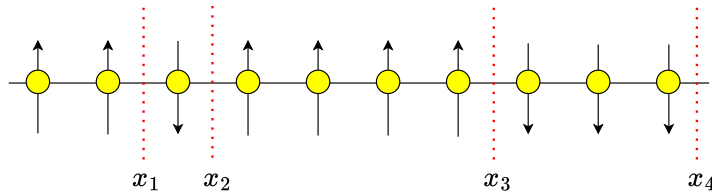


FIG. S1. A typical configuration of the ten-spin chain is used to explain the position of its domain wall x_1, x_2, \dots, x_N . We label the x_N by the spin in front of the domain wall.

After duality transformation the Hamiltonian becomes

$$\frac{1}{J_{XY}} H = - \sum_j (\tau_j^z \tau_{j+1}^z + \frac{1}{J_{XY}} \tau_j^x). \quad (\text{S7})$$

Therefore

$$\psi(s) \equiv \psi(\tau), \quad (\text{S8})$$

where τ is a bit string of τ^x . We can then rewrite the Hamiltonian in terms of Jordan-Wigner fermions:

$$\frac{1}{J_{XY}}H = -\sum_j (c_j^\dagger - c_j)(c_{j+1} + c_{j+1}^\dagger) - \frac{1}{J_{XY}}\sum_j (1 - 2c_j^\dagger c_j). \quad (\text{S9})$$

Here $\tau^x = 1 - 2n_j$. When $J_{XY} \rightarrow \infty$, this is the Majorana chain Hamiltonian, corresponding to the ferromagnetic state of the dual TFI model.

The ground state of the fermion model takes the following form:

$$\exp\left(\frac{1}{2}\sum_{ij} g_{ij}c_i^\dagger c_j^\dagger\right)|0\rangle, \quad (\text{S10})$$

where $|0\rangle$ is the empty state with $n_j = 0$ for all j , or $\tau_j^x = 1$. g_{ij} can be understood as the wavefunction of a Cooper pair. If there are N fermions at x_1, x_2, \dots, x_N , then

$$\psi(x_1, x_2, \dots, x_N) = \text{Pf } g_{x_i, x_j}. \quad (\text{S11})$$

In the direct product state representation of spins, x_1, x_2, \dots, x_N is the position of its domain wall (example see Fig. S1).

According to Eq.(S8) and (S10), $|\psi(s)|^2$ in Eq.(S5) is the value of the determinant as follows

$$\begin{vmatrix} 0 & g(x_1 - x_2) & \cdots & g(x_1 - x_N) \\ g(x_2 - x_1) & 0 & \cdots & g(x_2 - x_N) \\ \vdots & \vdots & \ddots & \vdots \\ g(x_N - x_1) & \cdots & g(x_N - x_{N-1}) & 0 \end{vmatrix} \quad (\text{S12})$$

where $g(x) = \frac{2}{L}\sum_{n=1}^{L/2}\left[\sin(kx)\sqrt{\frac{E(k)-\xi(k)}{E(k)+\xi(k)}}\right]$ in which L is the system size, $k = (2n-1)\pi/L$, $\xi(k) = -2\cos(k) + 2/J_{XY}$ and $E(k) = \sqrt{\xi^2(k) + 4\Delta^2 \sin^2 k}$.

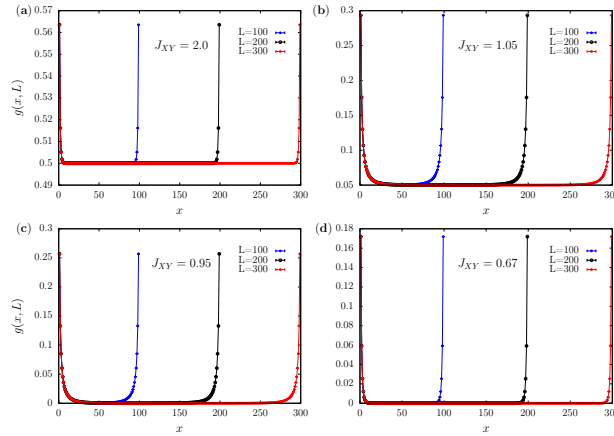


FIG. S2. Matrix element $g(x, L)$ in the PM (a)(b) or FM (c)(d) phase of the OH.

Since $\rho_A = e^{-H_E}$, $\langle s|e^{-H_E}|s\rangle = |\psi(s)|^2$ according to Eq.(S5). For arbitrary effective inverse temperature β_E of the EH H_E , we can derive the weight W_s of each $|s\rangle$ as $\langle s|e^{-\beta_E H_E}|s\rangle = |\psi(s)|^{2\beta_E}$. Using this weight, we can simulate the EH by MC method.

Notice that the physical meaning of the element $g(x)$ is similar to the energy cost between two domain walls with distance x on the Ising chain. As drawn in Fig. S2 (a) and (b), the $g(x)$ of different system size L , i.e., $g(x, L)$, has been plotted. As the size $L \rightarrow \infty$, ignoring the edge effect, the $g(x)$ in the bulk remains a finite value. It actually points to a long-range interaction of the Ising chain. Conversely, Fig. S2 (c) and (d) show the $g(x)$ in the bulk approaches to 0 which means a short-range interaction of the EH.

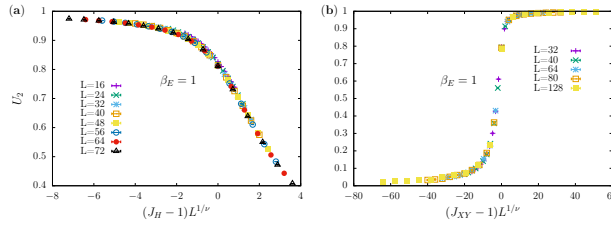


FIG. S3. Setting $\beta_E = 1$ and sweeping $J_H(J_{XY})$ near the critical point $J_c^P = 1$, the data of U_2 for different system sizes fall onto the same curve with $\nu = 1$.

The universality class at the critical points

We adopt finite-size scaling $A(g, L)L^\kappa = f[(g - g_c)L^{1/\nu}]$ to rescale the binder cumulant $A = U_2$ or squared magnetization $A = \langle(m^z)^2\rangle$, in which $\kappa = 0$ for $A = U_2$ and $\kappa = 2\beta/\nu$ for $A = \langle(m^z)^2\rangle$, $g = J_H(J_{XY})$ or $T_E = 1/\beta_E$ and ν is correlation length exponent.

As discussed in the main text, setting $\beta_E = 1$ and sweeping $J_H(J_{XY})$ near the critical point $J_c^P = 1$, the data of U_2 can be rescaled by 2D using universality class (UC) $\nu = 1$ see Fig. S3.

However, setting $J_H(J_{XY}) = 1$ and sweeping $T_E = 1/\beta_E$ near the critical point $\beta_E = 1$, the data of U_2 can not be rescaled by 2D using UC $\nu = 1$ see Fig. S4 (a). Set ν free to fit and we find that the data of U_2 can be rescaled by $1/\nu = 0.24(1)$ (see Fig. S4 (b)). Furtherly, we set $A = \langle(m^z)^2\rangle$ and $\kappa = 2\beta/\nu$ to fit ν and β/ν . We find that $\beta/\nu = 0.123(2)$ and $1/\nu = 0.34(2)$ can be used to rescale $\langle(m^z)^2\rangle$ for different system sizes, as shown Fig. S5.

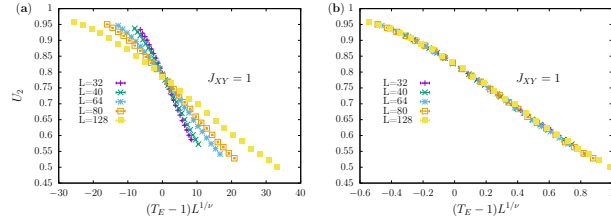


FIG. S4. Setting $J_{XY} = 1$ and sweeping $T_E = 1/\beta_E$ near the critical point $\beta_E = 1$, the data of U_2 for different system sizes can not fall onto the same curve with $\nu = 1$ (a) but can fall onto the same curve with $1/\nu = 0.24(1)$ (b).

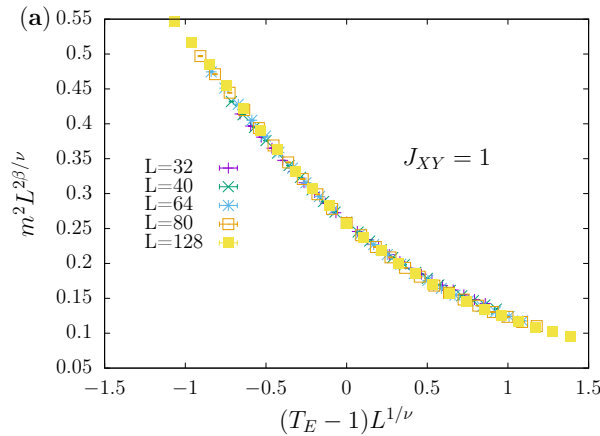


FIG. S5. Setting $J_{XY} = 1$ and sweeping $T_E = 1/\beta_E$ near the critical point $\beta_E = 1$, the data of $\langle(m^z)^2\rangle$ for different system sizes can fall onto the same curve with $1/\nu = 0.34(2)$ and $\beta/\nu = 0.123(2)$.

The Binder cumulant U_2 of the 1D ising model at the finite temperature

The Binder cumulant U_2 of the 1D ising model at the finite temperature is shown in Fig. S6.

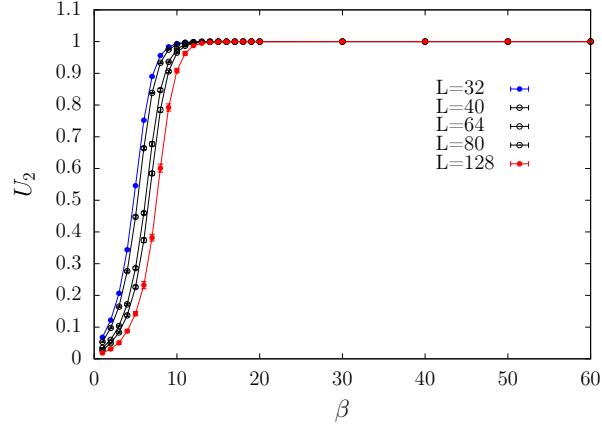


FIG. S6. The Binder cumulant U_2 of the 1D ising model at the finite temperature

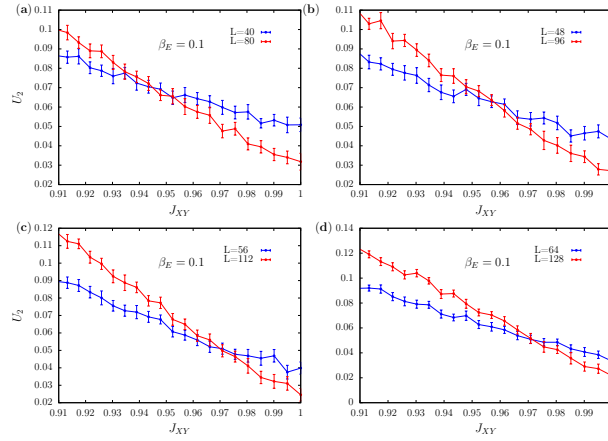


FIG. S7. The results of the U_2 for different $(L, 2L)$ vs J_{XY} setting $\beta_E = 0.1$.

Focus on the OH of the system H_{XY} in the FM phase

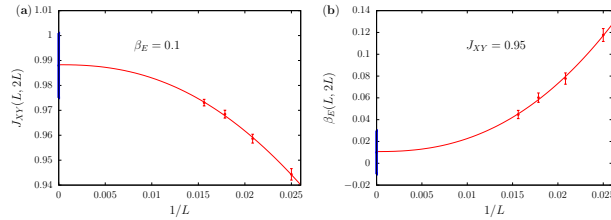


FIG. S8. (a) Fitting about the position of the crossing points of the U_2 curves setting $\beta_E = 0.1$. The blue symbol shows the extrapolated value at the thermodynamic limit, which is 1 within the error bar. (b) Fitting about the position of the crossing points of the U_2 curves setting $J_{XY} = 0.95$. The blue symbol shows the extrapolated value at the thermodynamic limit, which is 0 within the error bar.

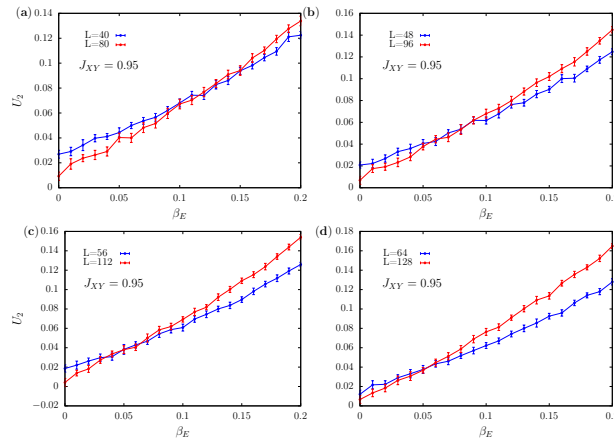


FIG. S9. The results of the U_2 for different $(L, 2L)$ vs β_E setting $J_{XY} = 0.95$.

As discussed in the main text for binder cumulant U_2 , the crossings of curves for different sizes drift towards to $J_{XY} = 1$ when we set the $\beta_E = 0.1$. Further, we show the results of the U_2 for different L and $2L$ in Fig. S7 and adopt the standard $(L, 2L)$ crossing analysis to do this. Fitting the crossing points of the curves for L and $2L$ (see Fig. S8) with

$$J_{XY}(L, 2L) = J_{XY}(L \rightarrow \infty) + aL^{-\omega}, \quad (\text{S13})$$

we find that $J_{XY}(L \rightarrow \infty)$ is 0.988(13) which is 1 within error bar.

Similarly, the results of the U_2 setting $J_{XY} = 0.95$ for different L and $2L$ are shown in Fig. S9. Fitting the crossing points of the curves for L and $2L$ (see Fig. S8) with

$$\beta_E(L, 2L) = \beta_E(L \rightarrow \infty) + aL^{-\omega}, \quad (\text{S14})$$

we find that $\beta_E(L \rightarrow \infty)$ is 0.01(2) which is 0 within error bar.

The details of replica quantum Monte Carlo method

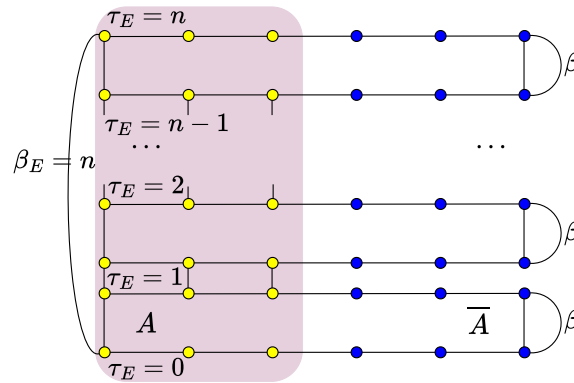


FIG. S10. The replica manifold structure in Rényi replica-partition-function $Z_A^{(n)}$. The replicas of entangling region A are glued together in the replica imaginary time direction and each replica of the environment region \bar{A} is independent in the imaginary time direction. Therefore, the imaginary time length for H_E is $\beta_E = n$ and that for total system H is $\beta = 1/T$.

Here, we introduce the details of replica quantum Monte Carlo method. As depicted in Fig. S10, $Z_A^{(n)}$ is a partition function in a replicated manifold, where the time-boundaries of area A of the n replicas are connected along imaginary

time and the time-boundaries of the area \bar{A} of every replica are independent to each other (each replica, the usual periodic boundary condition of β is maintained for sites in \bar{A}). It can be seen that the effective $\beta_E = n$ for the EH \mathcal{H}_E of the subsystem A is in the unit of 1 whereas the $\beta = 1/T$ of the total system is in the inverse unit of the physical energy scale of the original system, J of the Heisenberg model, for instance.

It's worth noting that there are two concepts of "temperature" above, one is the real temperature T ($1/\beta$) for the original Hamiltonian H , and the other one is the effective temperature T_E ($1/\beta_E$) for the EH \mathcal{H}_E . Here we set the β as large and let it grow as system size L to make the system approach its ground state. When we talk about the finite temperature phase transition of the EH \mathcal{H}_E , the "temperature" here means the T_E ($1/\beta_E$). In the replica manifold we simulated, the β_E can be tuned by changing the number of replicas n .
